Research Square

Preprints are preliminary reports that have not undergone peer review.
They should not be considered conclusive, used to inform clinical practice,
or referenced by the media as validated information.

Mixed layer and thermocline dynamics driving El Niño–La Niña modes since the middle Miocene

Anil Gupta

anilgupta021160@gmail.com

Indian Institute of Technology Kharagpur https://orcid.org/0000-0003-0536-3911

Ayushi Ram

Jacek Raddatz

GEOMAR Helmholtz Centre for Ocean Research Kiel https://orcid.org/0000-0002-5713-9682

Article

Keywords: Western Equatorial Pacific, El Niño–Southern Oscillation (ENSO), Thermocline Dynamics, Indonesian Gateway, Equatorial Undercurrent (EUC), Miocene-Pliocene Climate, Planktic Foraminifera, Stable Isotopes

Posted Date: June 9th, 2026

DOI: https://doi.org/10.21203/rs.3.rs-9863754/v1

License: This work is licensed under a Creative Commons Attribution 4.0 International License.
Read Full License

Additional Declarations: There is **NO** Competing Interest.

Abstract

The Western Equatorial Pacific (WEP) reigns the El Niño–Southern Oscillation (ENSO) dynamics through mixed layer – thermocline interactions and affects the ocean–atmosphere feedbacks in the tropics. To understand these dynamics, we present planktic foraminiferal relative abundance and stable isotope data from Ocean Drilling Program Site 803D since ~ 12.9 Ma to the Holocene. Our results reveal a transition of the WEP from a stratified warm pool state in the late middle Miocene to pronounced ENSO–like state during 8—7 Ma, and ultimately to a modern day West Pacific Warm Pool (WPWP) at ~ 2 Ma. Progressive shoaling of the thermocline led to enhanced surface productivity in the WEP at ~ 11 Ma, which subsequently promoted an El Niño–like mean state in the tropical Pacific at ~ 8 Ma. The sea level fall and progressive constriction of the Indonesian Gateway during the Late Miocene Cooling promoted the development of an oligotrophic WPWP and a switch to La Niña–like mean state at ~ 7 Ma. Such conditions closely resemble those established in the Pleistocene (since ~ 2 Ma), highlighting the late Miocene as an analogue to the modern ENSO state.

1. Introduction

Earth's climate system has witnessed a transition from a progressively cooler state since the late middle Miocene to the modern state, marked by a substantial decline in atmospheric pCO_2 (~ 200–350 ppm)[1]. This is associated with the major expansion of the East Antarctic Ice Sheet (EAIS) during the Middle Miocene Climate Transition (MMCT, ~ 14.6–13 Ma)[2,3]. Changes in the extratropical climate forcing likely influenced the mean state of the tropical Pacific and El Niño–Southern Oscillation (ENSO) variability, linking high-latitude climatic evolution with equatorial ocean–atmosphere dynamics[4].

Today, the tropical Pacific Ocean is characterized by a persistent Walker circulation, marked by easterly trade winds, rising air over the western equatorial Pacific (WEP) and sinking air over the eastern equatorial Pacific (EEP). This drives a pronounced west–east (zonal) asymmetry in sea surface temperature (SST) and thermocline structure, and is closely linked to the ENSO dynamics[5] (Fig. 1). As a result, the WEP hosts a thick warm mixed layer and a deep thermocline (> 150 m), whereas the EEP is characterized by a thinner mixed layer and a shallow thermocline[4] (~ 50 m) (Fig. 1). During the El Niño–state, the thermocline shoals in the WEP, associated with a weakened Walker circulation, which reverses during the La Niña –state when Walker circulation strengthens[4] (Fig. 1a, b). The efficiency of the Walker circulation is further tied to the depth and strength of the Equatorial Undercurrent (EUC), a narrow ~ 300 km wide eastward flowing subsurface current that shoals from ~ 200 m in the WEP to < 50 m in the EEP, closely following the zonal slope and vertical structure of the equatorial thermocline[6] (Fig. 1).

Since ~ 17 to 3 Ma, tectonic reorganization of the Indonesian Gateway and the Central American Seaway (Fig. 1), likely modulated equatorial Pacific climate through alternating La Niña– and El Niño–like states[7,8,9]. The northward drift of Australia progressively restricted the Indonesian Gateway from a deep interocean gateway to a shallow throughflow between the late Oligocene and Miocene, reducing Pacific–

Indian deep water exchange[8,9,10]. Similarly, progressive shoaling and restriction of the Central American Seaway from the middle Miocene to Plio–Pleistocene (~ 13–3 Ma) reduced Pacific-Caribbean exchange leading to major reorganizations of ocean circulation[11,12]. Coupled changes in the tropical seaways and Antarctic glaciation since the middle Miocene reorganized equatorial Pacific circulation, intensifying gyre systems, the Equatorial Counter Current and EUC, alongside the development of the West Pacific Warm Pool (WPWP)[5,8,13]. However, the extent to which intensification of the EUC influenced thermocline depth and vertical stratification in the WEP remains poorly constrained, with important implications for the emergence of ENSO-like variability.

Eventually, during the late Miocene, perturbations in the global carbon cycle, including the Late Miocene Biogenic Bloom (LMBB)[14,15] and the Late Miocene Carbon Isotope Shift (LMCIS) (~ 8–7 Ma), coincided with a prolonged cooling trend (~ 7–5.4 Ma) that strengthened meridional temperature gradients and likely intensified large-scale atmospheric circulation[15,16]. In contrast, the early Pliocene represents a markedly different state, characterized by reduced thermal gradients and a more El Niño-like mean climate[4]. This state was subsequently replaced after ~ 3.5–3 Ma by cooling of the upper ocean and shoaling of the thermocline in the WEP, linked to gateway constrictions and enhanced influence of extratropical waters[17]. However, whether comparable reorganizations of thermocline structure occurred during the Miocene and the Plio–Pleistocene and how these were modulated by evolving boundary conditions remains debatable.

To address this gap, we analysed sediment core samples from ODP Site 803D, located at 02° 25.98'N, 160° 32.46'E, and a water depth of 3412.2 m, on the northeastern margin of the Ontong Java Plateau in the WEP (Fig. 1b). This study aims to: (1) reconstruct the temporal evolution of the WEP since the late middle Miocene following the MMCT using planktic foraminiferal relative abundance and stable isotope data; (2) investigate the role of progressive constriction of the Indonesian Gateway and Central American Seaway in reshaping the vertical thermal structure of the WEP and facilitating the initial development of the WPWP and the intensification of EUC; (3) To identify intervals of ENSO–mode and to find out the tectonic and atmospheric drivers that forced the equatorial Pacific to shift from an El Niño–like state to a La Niña–dominated regime and vice versa. Our results demonstrate that late Miocene EUC intensification was driven by falling sea levels linked to EAIS growth coupled with the deep water restriction through the Indonesian Gateway. Similarly, the development of WPWP–like conditions during the Late Miocene Cooling (LMC) closely resembles those observed in the Pleistocene, suggesting that key features of tropical Pacific Ocean–atmosphere structure were already established during the late Miocene (~ 7 Ma).

2. Results

2.1. Stable oxygen and carbon isotope analysis

The oxygen isotope values of the mixed layer dwelling species *Trilobatus sacculifer* and upper thermocline dwelling taxa *Fohsella fohsi* and *Globorotalia menardii* provide key information about middle to late Miocene upper ocean variability at Site 803D (Fig. 2b, c). Between ~ 12.9 and 11.0 Ma, the $\delta^{18}O_{T. sacculifer}$ values remain negative with marked variability, averaging ~ – 0.80‰. In contrast, the upper thermocline dwelling species show a gradual enrichment in the $\delta^{18}O$ values over this interval (Fig. 2b, c). Specifically, $\delta^{18}O_{F. fohsi}$ (from ~ 12.9 to 12.07 Ma) and $\delta^{18}O_{G. menardii}$ (from ~ 12.07–11 Ma) increase progressively from − 0.42‰ to 0.68‰ (Fig. 2b). From ~ 11 to 8 Ma, the $\delta^{18}O_{G. menardii}$ values exhibit a marked decreasing trend, decreasing from 0.68‰ to − 1.015‰ (Fig. 2b). During the interval ~ 9.8 to 8 Ma, the $\delta^{18}O_{T. sacculifer}$ values show an average of − 1.20‰. Between ~ 8 and 7 Ma, $\delta^{18}O_{G. menardii}$ maintains relatively low values, averaging − 0.72‰. Subsequently, at ~ 7 Ma, both $\delta^{18}O_{T. sacculifer}$ and $\delta^{18}O_{G. menardii}$ display a progressive enrichment toward heavier values, continuing until ~ 6.5 Ma. Biostratigraphically, the Last Occurrence (LO) of *F. fohsi* is recorded at ~ 11.03 Ma, followed closely by the First Occurrence (FO) of *G. menardii* at ~ 12.07 Ma at ODP Site 803D.

The $\delta^{13}C$ values of *T. sacculifer* ($\delta^{13}C_{T. sacculifer}$), *G. menardii* ($\delta^{13}C_{G.menardii}$) and *F. fohsi* ($\delta^{13}C_{F. fohsi}$) show pronounced changes since the late Middle Miocene (Fig. 2d, e). An abrupt decrease in both the mixed layer species and thermocline species is observed between ~ 11 and 9.8 Ma. During this interval, the $\delta^{13}C_{T. sacculifer}$ decrease sharply from 3.2 to 0.26‰, while $\delta^{13}C_{G. menardii}$ values decrease from 1.98 to 1.09‰. Subsequently, between ~ 8 and 6.5 Ma, both records exhibit a gradual decrease. The $\delta^{13}C_{T. sacculifer}$ values decrease from ~ 2.60 to ~ 1.30‰, whereas those of $\delta^{13}C_{G. menardii}$ decrease from ~ 1.91 to ~ 0.9‰.

2.2. Trends in the mixed layer and thermocline species

According to habitat preferences, the planktic foraminiferal species are grouped into mixed layer and thermocline species (see Methods, Supplementary material and Supplementary Table S2). The major mixed layer species are *T. sacculifer*, *Dentoglobigerina altispira, Globigerinita glutinata, Paragloborotalia continuosa, Paragloborotalia mayeri, Paragloborotalia siakensis*, while the major thermocline dwelling species include *Globorotalia menardii, Fohsella fohsi, Neogloboquadrina dutertrei, Neogloboquadrina acostansis, Dentoglobigerina venezuelana.* Species with rare abundances are provided in Supplementary Table S2. Relative abundances of the thermocline species and mixed layer species are given in Fig. 3a, b. Between ~ 13 and 11 Ma, mixed layer species dominate the assemblage, averaging ~ 81%, whereas the thermocline species remain scarce. Afterwards, the relative abundance of mixed layer species decreases, remaining at an average of ~ 59% between ~ 11 and 8 Ma, whereas thermocline species increase having an average of ~ 41%. Between ~ 8 and 7 Ma, mixed layer species decrease sharply from ~ 59 to ~ 16%, accompanied by a marked rise in thermocline species from ~ 41% to ~ 84%. At ~ 7 Ma the mixed layer and thermocline converged, and since then this trend reversed, as mixed layer species gradually increase from ~ 16 to ~ 64% by ~ 6.2 Ma, whereas thermocline species decrease from ~ 84 to ~ 36% (Fig. 3).

3. Discussion

3.1. Enhanced stratification and thermocline deepening from ~ 13 to 11 Ma

Between ~ 13 and 11 Ma, the $\delta^{18}O_{T.\ sacculifer}$ values record short-term, episodic fluctuations in mixed layer of the WEP (Fig. 2c). In contrast, the thermocline species shows progressive $\delta^{18}O$ enrichment (Fig. 2b). This is consistent with the previous observations[5] reporting relatively positive $\delta^{18}O$ values in thermocline dwelling species (Fig. S2). Moreover, this interval shows a higher relative abundance of mixed layer species (Fig. 3b), whereas the relative abundance of thermocline species particularly *D. venezuelana* decrease steadily (Fig. 3a, d). The progressive enrichment in the $\delta^{18}O$ values of thermocline species, together with the dominance of mixed layer species, suggests enhanced upper-ocean stratification and a relatively deep thermocline at Site 803. Although thermocline species show stronger enrichment, both mixed layer and subsurface taxa display an overall shift toward heavier $\delta^{18}O$ values between ~ 13 and 11 Ma. As the benthic $\delta^{18}O$ record does not show a comparable trend (Fig. 4c), the planktic $\delta^{18}O$ enrichments likely reflect not only cooling but also salinity changes.

The MMCT represents a major stepwise intensification of global cooling, associated with the EAIS expansion and significant sea level fall[3,18]. Expansion of the EAIS likely enhanced the formation of intermediate and deep waters in the Southern Ocean, promoting increased northward penetration of Southern Component Intermediate Water into the Pacific thermocline[19,20]. Such high–low latitude coupling likely operated through subsurface “ocean tunnelling,” whereby extratropical mode and intermediate waters were advected equatorward and subsequently incorporated into the equatorial thermocline[7,21,22]. This process would have contributed to progressive cooling and freshening of tropical Pacific subsurface waters. However, despite the relatively low salinity of southern-sourced mode and intermediate waters[23], the progressive enrichment in the thermocline $\delta^{18}O$ values suggests that subsurface cooling associated with enhanced southern-sourced ventilation dominated over the influence of freshening on the $\delta^{18}O$ signal.

Concurrently, progressive uplift of the Panama restricted deep water exchange between the Pacific and Atlantic[11], while modelling studies suggest reduced Pacific outflow through the Central American Seaway was compensated by enhanced throughflow via the Indonesian Archipelago[24]. However, concurrent global sea level fall likely increasingly restricted Indonesian Gateway flow, reducing Pacific-Indian Ocean exchange and limiting warm water export from the WEP (Fig. 4d). Consistently, Sosdian and Lear[25] concluded that restriction of Indonesian Gateway flow following the MMCT led to warming of the WEP and concurrent freshening of the eastern tropical Indian Ocean. Additionally, Zhang et al.[26] reported a ~ 4°C warmer Pacific warm pool at ~ 12 Ma (Fig. 4e). Collectively, these processes enhanced upper ocean stratification in the WEP during the middle–late Miocene transition (~ 13–11 Ma), promoting initial development of the WPWP.

3.2. **Intensification of Equatorial Undercurrent (EUC) and emergence of an El Niño like mean state in the equatorial Pacific (~ 11–7 Ma)**

Since ~ 11 Ma, decreasing $\delta^{18}O_{G.\ menardii}$ values at Site 803D suggests prolonged upper thermocline warming (Fig. 2b). Concurrently, the relative abundance of the thermocline species increased markedly, whereas the mixed layer species decreased (Fig. 3a, b). Together these changes reflect the initiation of thermocline shoaling and mixed layer thinning, marking a clear transition relative to the thicker mixed layer state prevailing during ~ 13–11 Ma (Fig. 3a, b). This thermocline warming trend, however, was interrupted between ~ 10.4 and 9.8 Ma, when both the $\delta^{18}O_{T.\ sacculifer}$ and $\delta^{18}O_{G.\ menardii}$ values synchronously increased (Fig. 2b, c). This shift is most plausibly attributed to enhanced intrusion of extratropical mode waters into the WEP upper water column. Previous studies from the Indian Ocean also indicate an increasing influence of Southern Hemisphere sourced intermediate to deep waters during this interval, likely linked to strengthening of the Antarctic Circumpolar Current[20,27].

Bali et al.[28] proposed that progressive restriction of the Central American Seaway prior to ~ 9.5 Ma was a key driver for strengthened southern–sourced overturning circulation. Such high-latitude influence on tropical thermocline structure is further supported by early Quaternary records, which demonstrate that ocean tunnelling of southern-sourced subsurface waters into the equatorial Pacific drove freshening and cooling of the deep thermocline in phase with Antarctic ice sheet expansion[21,22]. We therefore infer that between ~ 10.4 and 9.8 Ma, enhanced penetration of cooler Southern Ocean waters into the Pacific caused a short–lived cooling as recorded in the $\delta^{18}O$ values of thermocline species.

Since ~ 9.8 Ma, the $\delta^{18}O_{G.\ menardii}$ values exhibit a sustained decrease (Fig. 2b). Concurrently, a distinct faunal transition occurred, marked by the first appearance of *Neogloboquadrina* spp. lineage at ~ 9.8 Ma. Additionally, the mixed layer dwelling *Paragloborotalia siakensis–Paragloborotalia mayeri* group records its last biostratigraphic occurrence at ~ 9.8 Ma. Together, these changes led to a decrease in the relative abundance of mixed layer species and increase in the thermocline species, indicating a progressive shoaling of the thermocline (Fig. 3a, b). The shoaling of the thermocline alongside decreases in the $\delta^{18}O$ values of thermocline species is consistent with the intensification of the EUC. This is likely driven by restriction of Pacific– Indian Ocean deep water exchange, which promoted warm water accumulation in the WEP (as discussed in the ~ 13–11 Ma interval) and the consequent development of an easterly return flow as the EUC[10, 19].

Enhanced EUC influence likely shoaled warm upper thermocline waters into the photic zone resulting in a thinner mixed layer and a vertically expanded thermocline in the WEP[13]. Accordingly, a sustained decrease in the $\Delta\delta^{18}O_{G.\ menardii\ -\ T.\ sacculifer}$ values since ~ 9.8 Ma at Site 803D indicate reduced interspecific difference in the $\delta^{18}O$ values between the mixed layer and the upper thermocline dwelling species (Fig. 2a). This is consistent with increased abundances of thermocline dwelling foraminifera, indicating progressive restriction of the Indonesian Gateway which led to warm surface water accumulation in the WEP. This process strengthened zonal pressure gradients and promoted

intensification of eastward-flowing EUC, accompanied by a shoaled thermocline. Together these changes indicate a shift towards the development of El Niño–like conditions.

Between ~ 11 and 9.8 Ma, the planktic foraminiferal assemblage shows a marked increase in the relative abundance of *G. glutinata*, a species associated with elevated surface productivity[29], concomitantly low abundances of *T. sacculifer*, a typical indicator of oligotrophic conditions in the WEP[30] (Fig. 3e, f). In parallel, the $\delta^{13}C$ values of both mixed layer and thermocline species exhibit a pronounced decrease since ~ 11 Ma (Fig. 2d, e). Together, these evidences indicate elevated surface productivity in the WEP upper water column. The subsequent appearance and gradual increase of *Neogloboquadrina* spp. at ~ 9.8 Ma suggests increasing thermocline productivity (Fig. 3c). We infer that the eutrophic conditions were established in the WEP at ~ 11 Ma, marking the onset of enhanced regional productivity. This shift coincides with the Late Miocene Biogenic Bloom (LMBB), a recognized interval of globally elevated marine productivity[31,32]. The LMBB has been widely attributed to various factors viz. increased global nutrient availability driven by factors such as altered oceanic and atmospheric circulation[33], gradual shoaling of the Central American Seaway[34], initiation of the Indian Monsoon System[31], and enhanced riverine input from mountain uplift[35].

Recent results from WEP Site U1488 constrain onset of the LMBB at ~ 8.1 Ma, based on increased carbonate mass accumulation rates[36] (Fig. S2), in agreement with records from the EEP and South Atlantic[15,16,37]. Further, foraminiferal mass accumulation rates (MAR) at ODP Site 803D remained high between ~ 9.8 and 8 Ma, compared to younger intervals[38] (Fig. S2). A comparable increase in productivity has been reported between ~ 9.0 and 8.8 Ma as the initial phase of the widespread biogenic bloom[5]. Our record, however suggests that enhanced productivity in the WEP began earlier, at ~ 11 Ma, which we attribute to progressive thermocline shoaling associated with Indonesian Gateway restriction, which enhanced upward nutrient flux into the euphotic zone. In contrast, the later intervals likely represent fully developed expression of the LMBB at regional to global scales. These observations suggest that regional oceanographic processes, particularly thermocline dynamics and associated changes in surface circulation likely influenced the initiation and modulation of the expression of LMBB in the WEP. Our proposed timing of enhanced productivity in the WEP roughly corresponds with other regional records from the South China Sea (SCS)[39], where increased nutrient supply linked to strengthening of the East Asian Summer Monsoon has been inferred since ~ 12 Ma. This pattern suggests that the early development of elevated productivity in the WEP may have formed part of a wider regional response to changing nutrient regimes and oceanographic reorganization.

The shallowing of the Indonesian Gateway increasingly influenced upper ocean structure in the WEP. This reorganization coincides with the upper thermocline warming at Site 803D, which intensified through time as indicated by the minimum $\delta^{18}O$ values at ~ 8 Ma (Fig. 2b). These changes suggest reduced thermal stratification associated with thermocline shoaling and enhanced vertical mixing (Fig. 2b, c). Subsequently, between ~ 8 and 7 Ma, the $\Delta\delta^{18}O_{\textit{G. menardii} - \textit{T. sacculifer}}$ values decreased, reflecting persistence of a shoaled thermocline and a thinner mixed layer (Fig. 2a). Planktic foraminiferal

assemblages mirror this shift, with decreasing relative abundance of mixed layer species (*T. sacculifer*, *G. glutinata*) (Fig. 3e, f) and increasing thermocline species particularly *D. venezuelana* and *Neogloboquadrina* spp. (Fig. 3c, d). Together, this ecological changes support emergence of an El Niño–like mean state across the equatorial Pacific consistent with the gradual thermocline shoaling in the WEP driven by tectonic reorganization. This mean state, established between ~ 8 and ~ 7 Ma, likely developed under relatively open Indonesian Gateway following global sea level rise[40,41] (Fig. 4d). The interval was also characterised by weakened trade winds, a southward shift in Hadley circulation, and reduced meridional SST gradients[15,16].

Elevated abundances of phytodetritus-exploiting benthic foraminifera species and high carbonate MARs at Site U1488 in the WEP during this time indicate intensified nutrient supply[36] (Fig S2). This was likely linked to enhanced EUC-driven upwelling consistent with the El Niño–like conditions. A shoaled thermocline north of New Guinea enhanced the ability of the EUC to entrain and transport iron-rich shelf sediments. Intensification of the New Guinea Coastal Undercurrent (NGCUC) increased dissolved iron supply to surface waters, stimulating phytoplankton growth[42]. The EUC therefore acted as a critical conduit for micronutrient delivery and enhanced surface productivity[43]. Concurrent increases in *Neogloboquadrina* spp. abundance and reduced upper ocean $\delta^{13}C$ gradients at nearby ODP Site 806 further support a regional productivity enhancement driven by thermocline shoaling[5]. Furthermore, the resumption of carbonate accumulation in the equatorial Pacific since ~ 8 Ma likely reflects enhanced surface productivity[44]. The development of El Niño–like conditions corresponds with a subdued South Asian summer monsoon between ~ 11 and 7 Ma[45], reflecting reduced convection over the WEP and a weakened Walker circulation.

Additionally, our planktic $\delta^{13}C$ records exhibit notable decreases of ~ 0.8‰ between ~ 7.8 and 6.5 Ma which is consistent with major negative shift in both benthic and planktic foraminiferal $\delta^{13}C$ in all ocean basins, the so-called LMCIS[5,46,47,48] (Fig. 2d, e). The partial temporal overlap between the LMBB and LMCIS might suggest a link between enhanced marine productivity and global carbon cycle reorganization. Vincent et al.[49] proposed that the shift toward lower $\delta^{13}C$ values reflects the addition of ^{12}C enriched organic matter into the ocean, derived from erosion and remobilization of organic matter during regression associated with sea level fall. However, the longer duration of the LMBB relative to the LMCIS indicate productivity changes alone are insufficient to explain the scale and rate of the transition[14]. Instead, changes in ocean circulation likely shifted the balance of different deep water sources, affecting the $\delta^{13}C$ values[32]. Thus, distinct timings of the LMBB and LMCIS at Site 803D highlights the role of different forcing factors driving the two events.

3.2. Shift from an El Niño–like to a La Niña–like mean state during ~ 7–5.2 Ma

From ~ 7 to 5.2 Ma, both the $\delta^{18}O_{T.\ sacculifer}$ and $\delta^{18}O_{G.\ menardii}$ values gradually increased, indicating progressive upper water column cooling in our study area. This trend is consistent with the LMC, a global

cooling phase linked to declining atmospheric pCO_2 below ~ 280 ppm, likely driven by intensified rock weathering and reorganisation of ocean circulation[16,33,46] (Fig. 4f). Comparable cooling trends are documented across the Pacific, Atlantic, Indian Oceans, and Mediterranean and South China Sea as well as WEP where SSTs declined below early Pliocene values during the LMC[15,46,47,50] (Figs. 4e and S2). The magnitude of cooling varied with latitude, reaching up to ~ 8°C in high-latitude regions, compared to more moderate decreases of ~ 2–4°C in tropical and subtropical settings, increasing meridional temperature gradient[15,16,46]. In parallel, planktic foraminiferal assemblages at our site exhibit a pronounced shift towards increasing relative abundance of the mixed layer species (Fig. 3b), particularly *T. sacculifer* (Fig. 3e), whereas thermocline species including *D. venezuelana* and *Neogloboquadrina* spp. decrease significantly (Fig. 3c, d). Together, these patterns indicate a progressive thickening of the mixed layer in the WEP during the pervasive LMC, along with oligotrophic surface-water conditions. Such scenario is consistent with a La Niña–like mean state and marks the beginning of the development of WPWP. Further, the WEP was characterized by enhanced upper ocean stratification and reduced nutrient supply to the surface ocean. The onset of La Niña–like state coincides with intensification of the South Asian monsoon[45], suggesting a close climatic link.

Notably, records from Site U1488 also indicate a distinct La Niña–like phase between ~ 6.2 and 5.5 Ma[36]. Similarly, reduced surface productivity is also observed at ODP Site 806 in the WEP, where declining radiolarian and *Neogloboquadrina* spp. abundances after ~ 7.2 Ma have been reported[5], consistent with reduced nutrient supply under increasingly stratified, oligotrophic conditions. We therefore infer that expression of the LMBB in our study area was dampened during this interval with the development of oligotrophic conditions in the upper water column of the WEP.

Drury et al.[15] linked restriction of the Central American Seaway and Indonesian Gateway to the development of an asymmetric equatorial Pacific mean state, with EEP cooling, stronger trade winds, enhanced upwelling, and larger zonal $\delta^{18}O$ and SST gradients (Fig. 4e). Prolonged low sea level conditions between ~ 7 and 5 Ma (Fig. 4d)[41], likely linked to development of ephemeral northern hemisphere glaciation (NHG) ~6–5.5 Ma[46] (from global benthic data; Fig. 4c). This may have further restricted Indonesian Gateway transport; promoting retention of warm surface waters in the WEP. Such restriction likely enhanced thermocline asymmetry across the equatorial Pacific, strengthening the Walker circulation. Similarly, stronger upwelling and increased productivity in the EEP between ~ 7 and 5 Ma has been reported by Seki et al.[51]. Together, these observations suggest enhanced basin-wide thermocline tilting, deepening the thermocline in the WEP, reinforcing a warm pool and oligotrophic conditions.

3.3. Permanent El Niño-like condition during the early Pliocene (~ 5.2 to 3.5 Ma):

Between ~ 5.2 and 3.5 Ma, both the $\delta^{18}O_{\textit{T. sacculifer}}$ and $\delta^{18}O_{\textit{G. menardii}}$ values decreased markedly, indicating warming in both mixed layer and thermocline in the WEP[17] (Fig. 2b, c). Consistently, the

relative abundance of mixed layer species, particularly *T. sacculifer* decrease notably, coupled with an increase in thermocline dwelling species, particularly *D. venezuelana*. Together, these trends indicate thermocline shoaling and mixed layer thinning during the early Pliocene (Fig. 3a, b, d, e). We interpret this as a shift from a warm pool state with a relatively thick mixed layer during the LMC to an expanded warm pool characterized by a thinner mixed layer during the early Pliocene. This configuration is consistent with elevated SSTs in the Pacific[4]. Such conditions have been linked to a permanent El Niño–like state in the tropical Pacific, characterized by reduced zonal SST gradients and weakened Walker circulation during the early Pliocene[4]. However, subsequent proxy records suggest that zonal temperature gradients between the eastern and western tropical Pacific persisted during this interval, supporting a more modern-like ("El Padre") Pacific mean state rather than a fully developed permanent El Niño[26,52,53]. During this time, global mean temperature was ~ 1 to 5°C higher than today[54] with atmospheric CO_2 concentrations near or slightly above modern values[54,55] (365–415 ppm; Fig. 4f).

Retreat of the Antarctic ice sheet during the early Pliocene reduced global ice volume[40] resulting in eustatic sea levels ~ 25 m higher than Present[41,56] (Fig. 4d). Concurrently, reduced SST contrast between WEP and EEP[4,57], reinforced weakened Walker circulation. In parallel, a substantially reduced equator to subtropical meridional temperature gradient implies weakened HC and trade winds[58]. This is consistent with the humid conditions over northwest Australia and diminished coastal upwelling[59]. Proxy records from the Chinese Loess Plateau indicate a strengthened East Asian Summer Monsoon and weakened Winter Monsoon during the Pliocene[60], supporting modified land-sea thermal contrast under a warmer tropical Pacific mean state.

3.4. Plio-Pleistocene cooling in the WEP (~ 3.5 to 2.2 Ma)

Subsequently, at ~ 3.8 Ma, the relative abundance of thermocline species sharply increased at Sits 803D (Fig. 3b), whereas mixed layer species *T. sacculifer* decreased (Fig. 3a, e). The faunal reorganization likely reflects marked thermocline shoaling and enhanced productivity in the WEP[61]. At ~ 3.5 Ma, increased $\delta^{18}O$ values in both taxa mark the onset of sustained cooling, linked to Southern Hemisphere ice sheet expansion and incursion of Subantarctic Mode Water from the Southern Ocean into the WEP thermocline[17]. The near-synchronous constriction of the Indonesian Gateway likely restricted export of these southern-sourced waters into the Indian Ocean, enhancing their retention within the western Pacific[7]. Subsequent entrainment into the EUC may have facilitated eastward transport, influencing thermocline conditions across the tropical Pacific[61]. Kimble and Herbert[62] also concluded the changes in temperature and nutrient conditions of the mid-latitude waters ventilating the tropical Pacific via ocean tunnelling process, caused stronger late Pliocene surface productivity gradient in the EEP relative to today. At ~ 3 Ma, global climate underwent major reorganization, during the time of continued Central American Seaway closure and onset of the NHG[12]. Increased Southern Ocean stratification at ~ 3 Ma may have reduced ocean–atmosphere CO_2 exchange, contributing to declining atmospheric CO_2 levels (from 310 to 245 ppm) and global cooling during the Plio–Pleistocene transition[54,63,64]. Consequently,

WEP cooling, initiated at ~ 3.5 Ma intensified between ~ 3 and 2.2 Ma[17]. During this interval, the decreasing $\Delta\delta^{18}O_{G.\ menardii\ -\ T.\ sacculifer}$ values indicate reduced isotopic contrast between the thermocline and mixed layer, reflecting mixed layer cooling as $\delta^{18}O$ values of *T. sacculifer* approached those of *G. menardii* (Fig. 2a). A similar reduction in $\Delta\delta^{18}O$ values occured during the late Miocene (See section 3.2), which resulted from subsurface warming, driven by decreasing $\delta^{18}O$ of *G. menardii*.

At ~ 3 Ma, tectonic reorganization of the Indonesian Gateway, associated with the northward migration of New Guinea restricted throughflow and shifted its source from warm South Pacific to cooler North Pacific waters[65]. This caused mixed layer thickening simultaneous with surface cooling in the equatorial Pacific[7,17]. In contrast, late Miocene thermocline warming and shoaling was coupled with mixed layer thinning, linked to intensified EUC following deep Indonesian Gateway restriction. Although both intervals exhibit reduced vertical $\delta^{18}O$ gradients, these reflect fundamentally different oceanographic states driven by contrasting surface and subsurface processes. Thereafter, large sea level fall over the past ~ 2.7 Ma indicates major expansion of Northern Hemisphere ice sheets during the Quaternary[41] (Fig. 4d).

3.5. Strengthening of the West Pacific Warm Pool (WPWP) at ~ 2.2 Ma

At ~ 2.2 Ma, a concurrent decrease in $\delta^{18}O$ values of *T. sacculifer* and increase in $\delta^{18}O$ values of *G. menardii* mark mixed layer warming simultaneous with upper thermocline cooling, reflecting the strengthening of vertical thermal stratification[17] (Fig. 2b, c). The progressively increasing $\Delta\delta^{18}O_{G.\ menardii\ -\ T.\ sacculifer}$ values also indicate the onset of thickening of the mixed layer at Site 803D (Fig. 2a).

Since ~ 2 Ma, the $\delta^{18}O$ values of *T. sacculifer* and *G. menardii* at Site 803D exhibit synchronous trends, signalling stabilization of the vertical thermal gradient in the WEP and marking further strengthening of the WPWP[17] (Fig. 2b, c). This transition coincided with a sharp increase in mixed layer species abundance, with *G. ruber* becoming dominant, indicating a thickened mixed layer and oligotrophic conditions[17]. These changes reflect intensified Walker circulation driven by stronger easterlies, enhancing upwelling and productivity in the EEP and heat accumulation in the WEP[51], following the strengthening of NHG. Intensification of the global atmospheric circulation and equatorward migration of the trade winds at ~ 2 Ma[66] likely contributed to reduced Indonesian Gateway surface water transport[67].

Climate model results indicate that reduced transport through the Indonesian Gateway enhances precipitation over the WEP at the expense of the eastern Indian Ocean and northwest Australia, promoting warmer, drier conditions over northern Australia[68]. Pronounced Antarctic ice sheet expansion and cooling of high- to mid-latitude surface waters ~ 1.5 Ma, were accompanied by a marked increase in Southern Ocean dust and iron flux[69]. Concurrently, WPWP records show enhanced thermocline to deep-thermocline temperature variability, freshening, and increased influence of southern-sourced subsurface

waters between ~ 1.7 and ~ 1.2 Ma, suggesting intensified oceanic tunnelling of extratropical waters into the tropical Pacific[21,22].

4. Conclusions

This study unravels significant transitions in the evolution of the western equatorial Pacific (WEP) since late middle Miocene, which is governed by coupled process of cryosphere driven sea level change, ocean gateway constriction, and ocean–atmosphere dynamics. Between ~ 13 and 11 Ma, Antarctic ice sheet expansion and progressive restriction of the Indonesian Gateway promoted warm surface water accumulation in the WEP, strengthening the strong upper ocean stratification. This, in turn, facilitated intensification of the Equatorial Undercurrent (EUC) at ~ 9.8 Ma. A progressive thermocline shoaling and warming during ~ 9.8 to 8 Ma led to an El Niño–like state in the equatorial Pacific. Subsequently, an oligotrophic West Pacific Warm Pool (WPWP) was established during the Late Miocene Cooling (LMC, 7–5.2 Ma) accompanied by a transition of the equatorial Pacific toward a La Niña–like mean state. With the initiation of global warmth and rising sea level during the early Pliocene, the thermocline in our study area became shallow and Permanent El Niño–like mean state in the equatorial Pacific was established at ~ 5.2 Ma. Subsequently, with the strengthening of the Northern Hemisphere Glaciation during the Plio-Pleistocene, WPWP strengthened at ~ 2 Ma. Our results reveal development of the WPWP during the LMC, closely resembling those observed in the Pleistocene, thereby positioning the late Miocene as an analogue to Pleistocene climate variability. Further, our findings highlight that thermocline dynamics exert a significant influence on the long term shifts in the El Niño–Southern Oscillation (ENSO) since the late middle Miocene (~ 12.9 Ma), which modulates global heat distribution, monsoon dynamics, and tropical–extratropical climate linkages under changing boundary conditions.

Methods

Age model

The Age-Depth model for ODP Site 803, Hole D was derived from both paleomagnetic and biostratigraphic datums from the Initial Reports of ODP Leg 130[70] (Fig. S1). Age of each sample was calculated from 10 well preserved chron and subchron boundaries and 10 nannofossil datums (See supplementary material Table S1)[70], which were updated using the revised timescale[71]. The depth–age relationship is presented in Supplementary Fig S1.

Stable isotope analysis

For the stable oxygen and carbon isotope analyses, we used about 10–15 individuals of mixed layer dwelling planktic foraminifer *Trilobatus sacculifer* (250–350 µm) between ~ 12.90 Ma and ~ 6.5 Ma, comprising a total of 168 samples. Additionally, we analysed thermocline dwelling planktic foraminifer *Globorotalia menardii* (about 7–8 individuals from 250 – 350 µm) between ~ 12.07 Ma and ~ 6.5 Ma, and *Fohsella fohsi* (about 7–8 individual from 250–350 µm) between ~ 12.90 Ma and 12.07 Ma, comprising a

total of 193 samples. Samples correspond to an average temporal resolution of approximately 30–40 kyr per sample based on the age model. Published isotope data ($\delta^{18}O$ and $\delta^{13}C$) from Site 803D were used for the interval younger than ~ 6.5 Ma[17].

Stable oxygen and carbon isotope values of *G. menardii*, and *T. sacculfier*, *F. fohsi* specimens from ~ 12.90 Ma to ~ 6.5 Ma were analysed on a Thermo Scientific MAT253 Mass Spectrometer equipped with a CARBO Kiel IV device at GEOMAR, Germany. Isotope ratios were calibrated against in-house "Standard-Bremen" (Solnhofen limestone) that is in turn calibrated against the NBS 19 (National Bureau of Standards). The values are reported relative to the Vienna Pee Dee Belemnite (VPDB) standard and given in the common delta notation. The external reproducibility based on the in-house standard is ± 0.03‰ for $\delta^{13}C$ and ± 0.06‰ for $\delta^{18}O$ (1σ).

Counting of planktic foraminifera

Sediment samples were obtained from ODP Site 803D (02° 25.98'N, 160° 32.46'E, and a water depth of 3412.2 m), on the northeastern margin of the Ontong Java Plateau in the WEP (Fig. 1). Samples were provided by the International Ocean Drilling Programme (IODP) repository under IODP Request nos. 092064IODP; 105464IODP. Census counts of planktic foraminifera were made from 340 sediment core samples from ODP Site 803D, at an average temporal resolution of ~ 35000 years per sample. A total of 63 planktic foraminiferal species were identified following the established taxonomic criteria[72,73,74]. Planktic foraminiferal relative abundances were calculated following the methodology of Gupta and Thomas[75], involving the counting of ~ 300 specimens from the size fraction > 149 µm for each sample. The ecological preferences of planktic foraminiferal species were determined based on depth stratification of species assemblages in the water column[5,76,77,78]. According to their habitat preferences, the species were grouped into mixed layer species (MLS) and thermocline species (TCS) (Supplementary Table S2). The relative abundances of MLS and TCS were calculated by adding the relative abundance of all individual species based on the studies[79,80,81]. Key members of the MLS include *Globigerinoides ruber*, *Globigerinoides extremus*, *Globigerinoides obliquus*, *Trilobatus sacculifer*, *Globigerinoidesella fistulous*, *Globigerinoides conglobatus*, *Globigerina bulloides*, *Globigerina falconensis*, *Globoturborotalita apertura*, *Globoturborotalita rubenscens*, *Globoturborotalita. nepenthes*, *Orbulina universa*, *Globigerinita glutinata*, *Dentoglobigerina altispira*, *Dentoglobigerina globosa*, *G Globoturborotalita woodii*, *Globoturborotalita decorperta, Orbulina suturalis*. Major representatives of the TCS consist of *Globorotalia menardii*, *Globorotalia limbata*, *Globorotalia multicamerata*, *Globorotalia truncatulinoides*, *Globorotalia tosaensis*, *Globorotalia crassaformis*, *Globorotalia ungulata*, *Globorotalia margaritae, Globorotaliatumida*, *Globorotalia plesiotumida*, *Globorotalia hirsuta*, *Globorotalia scitula*, *Neogloboquadrina incompta*, *Neogloboquadrina pachyderma*, *Neogloboquadrina dutertrei*, *Neogloboquadrina humerosa*, *Neogloboquadrina acoestaensis*, *Neogloboquadrina inglei, Pulleniatina obliquiloculata*, *Pulleniatina primalis*, *Pulleniatina praecursor, Pulleniatina spectabilis, Globigerinella calida*, *Globigerinella siphonifera*, *Sphaeroidinella dehiscens*, *Sphaeroidinella praedehiscens*, *Sphaeroidinellopsis seminulina, Globigerinella obesa, Globoquadrina conglomerata, Globorotaloides hexagonus, Dentoglobigerina venezuelana,,*

Globoquadrina dehiscens, Dentoglobigerina baroemoenensis, Beella digitata, Beella praedigitata. Further details are provided in Supplementary material.

Completion of palaeo-CO_2 data

In Fig. 4f. paleo-CO_2 data derived from boron isotope methods range from ~ 13 Ma to the Holocene. We have used latest available datasets for each method, obtained from https://paleo-co2.org. Boron isotope-based estimates are palaeo-CO_2 estimates represented by blue diamonds[82,83,84,85,86,87]

Declarations

Data availability

All the data generated from ODP Site 803D are presented in this paper are available via the Zenodo database https://doi.org/10.5281/zenodo.20398141.

Acknowledgements

Authors thank Ocean Drilling Program for providing samples for the present study (IODP Request nos. 092064IODP; 105464IODP). AKG thanks the Anusandhan National Research Foundation (earlier SERB), Department of Science and Technology (DST), Government of India for Sir J.C. Bose fellowship (JBR/2021/000019). AR expresses her gratitude to DST, New Delhi for providing the INSPIRE Fellowship (IF190593). AR also thanks A.D. Singh, Banaras Hindu University Varanasi for his assistance in the identification of planktic foraminifera. GEOMAR Helmholtz Centre for Ocean Research Kiel, Wischhofstr. 1-3, D-24148, Kiel, Germany is acknowledged for providing stable isotope analysis facility. AR thanks Rudra Narayan Mohanty for providing valuable comments during the course of write-up of this manuscript.

Author information

Authors and Affiliations

Department of Geology and Geophysics, Indian Institute of Technology Kharagpur, Kharagpur, India

Ayushi Ram and Anil K. Gupta

GEOMAR Helmholtz Centre for Ocean Research Kiel, Wischhofstr. 1-3, D-24148, Kiel, Germany

Jacek Raddatz

Author contributions

Ayushi Ram: Writing – original draft, Validation, Methodology, Investigation, Formal analysis, Data curation, Conceptualization. Anil K. Gupta: Conceptualization, Formal analysis, Funding acquisition,

Investigation, Methodology, Resources, Supervision, Writing – original draft. Jacek Raddatz: Formal analysis, Resources, Methodology, Editing original draft.

Declaration of Competing Interest

The authors declare that they have no known competing financial interests or personal relationships that could have appeared to influence the work reported in this paper.

References

1. LaRiviere, J. P., Ravelo, A. C., Crimmins, A., Dekens, P. S., Ford, H. L., Lyle, M. & Wara, M. W. Late Miocene decoupling of oceanic warmth and atmospheric carbon dioxide forcing. *Nature* 486, 97–100 (2012). https://doi.org/10.1038/nature11200
2. Holbourn, A., Kuhnt, W., Kulhanek, D. K., Mountain, G., Rosenthal, Y., Sagawa, T. *et al.* Re-organization of Pacific overturning circulation across the Miocene Climate Optimum. *Nat. Commun.* 15, 8135 (2024). https://doi.org/10.1038/s41467-024-52516-x
3. Steinthorsdottir, M., Coxall, H. K., De Boer, A. M., Huber, M., Barbolini, N., Bradshaw, C. D. *et al.* The Miocene: the future of the past. *Paleoceanogr. Paleoclimatol.* 36, e2020PA004037 (2021). https://doi.org/10.1029/2020PA004037
4. Wara, M. W., Ravelo, A. C. & Delaney, M. L. Permanent El Niño-like conditions during the Pliocene warm period. *Science* 309, 758–761 (2005). https://doi.org/10.1126/science.1112596
5. Nathan, S. A. & Leckie, R. M. Early history of the Western Pacific Warm Pool during the middle to late Miocene (~ 13.2–5.8 Ma): role of sea-level change and implications for equatorial circulation. *Palaeogeogr. Palaeoclimatol. Palaeoecol.* 274, 140–159 (2009). https://doi.org/10.1016/j.palaeo.2009.01.007
6. Toggweiler, J. R., Dixon, K. & Broecker, W. S. The Peru upwelling and the ventilation of the South Pacific thermocline. J. Geophys. Res. Oceans 96, 20467–20497 (1991). https://doi.org/10.1029/91JC02063
7. Karas, C., Nürnberg, D., Gupta, A. K., Tiedemann, R., Mohan, K. & Bickert, T. Mid-Pliocene climate change amplified by a switch in Indonesian subsurface throughflow. *Nat. Geosci.* 2, 434–438 (2009). https://doi.org/10.1038/ngeo520
8. Kennett, J. P., Keller, G. & Srinivasan, M. S. Miocene planktonic foraminiferal biogeography and paleoceanographic development of the Indo-Pacific region. (1985). http://doi.org/10.1130/mem163-p197
9. Kuhnt, W., Holbourn, A., Hall, R., Zuvela, M. & Käse, R. Neogene history of the Indonesian throughflow. In *Continent-Ocean Interactions within East Asian Marginal Seas* (ed. Clift, P. *et al.*) *Geophys. Monogr.* 149, 299–320 (2004). https://doi.org/10.1029/149GM16
10. Hall, R. Cenozoic geological and plate tectonic evolution of SE Asia and the SW Pacific: computer-based reconstructions, model and animations. *J. Asian Earth Sci.* 20, 353–431 (2002).

https://doi.org/10.1016/S1367-9120(01)00069-4

11. Duque-Caro, H. Neogene stratigraphy, paleoceanography and paleobiogeography in northwest South America and the evolution of the Panama Seaway. *Palaeogeogr. Palaeoclimatol. Palaeoecol.* 77, 203–234 (1990). https://doi.org/10.1016/0031-0182(90)90178-A
12. Haug, G. H. & Tiedemann, R. Effect of the formation of the Isthmus of Panama on Atlantic Ocean thermohaline circulation. Nature 393, 673–676 (1998). https://doi.org/10.1038/31447
13. Hodell, D. A. & Vayavananda, A. Middle Miocene paleoceanography of the western equatorial Pacific (DSDP Site 289) and the evolution of *Globorotalia* (*Fohsella*). *Mar. Micropaleontol.* 22, 279–310 (1993). https://doi.org/10.1016/0377-8398(93)90019-T
14. Diester-Haass, L., Billups, K. & Emeis, K. C. In search of the late Miocene–early Pliocene "biogenic bloom" in the Atlantic Ocean (Ocean Drilling Program Sites 982, 925, and 1088). *Paleoceanography* 20, PA4001 (2005). https://doi.org/10.1029/2005PA001139
15. Drury, A. J., Lee, G. P., Gray, W. R., Lyle, M., Westerhold, T., Shevenell, A. E. & John, C. M. Deciphering the state of the late Miocene to early Pliocene equatorial Pacific. *Paleoceanogr. Paleoclimatol.* 33, 246–263 (2018). https://doi.org/10.1002/2017PA003245
16. Herbert, T. D., Lawrence, K. T., Tzanova, A., Peterson, L. C., Caballero-Gill, R. & Kelly, C. S. Late Miocene global cooling and the rise of modern ecosystems. *Nat. Geosci.* 9, 843–847 (2016). https://doi.org/10.1038/ngeo2813
17. Ram, A., Gupta, A. K. & Sanyal, P. Reconstructing evolution of the western Equatorial Pacific and its thermocline dynamics since the latest Miocene. *Glob. Planet. Change* 253, 104939 (2025). https://doi.org/10.1016/j.gloplacha.2025.104939
18. Holbourn, A., Kuhnt, W., Frank, M. & Haley, B. A. Changes in Pacific Ocean circulation following the Miocene onset of permanent Antarctic ice cover. *Earth Planet. Sci. Lett.* 365, 38–50 (2013). https://doi.org/10.1016/j.epsl.2013.01.020
19. Flower, B. P. & Kennett, J. P. Middle Miocene deepwater paleoceanography in the southwest Pacific: relations with East Antarctic Ice Sheet development. *Paleoceanography* 10, 1095–1112 (1995). https://doi.org/10.1029/95PA02022
20. Holbourn, A., Kuhnt, W., Clemens, S., Prell, W. & Andersen, N. Middle to late Miocene stepwise climate cooling: evidence from a high-resolution deep water isotope curve spanning 8 million years. *Paleoceanography* 28, 688–699 (2013). https://doi.org/10.1002/2013PA002538
21. Raddatz, J., Nürnberg, D., Tiedemann, R. & Rippert, N. Southeastern marginal West Pacific Warm Pool sea-surface and thermocline dynamics during the Pleistocene (2.5–0.5 Ma). *Palaeogeogr. Palaeoclimatol. Palaeoecol.* 471, 144–156 (2017). https://doi.org/10.1016/j.palaeo.2017.01.024
22. Raddatz, J., Zeeden, C., Kniest, J. F. & Nürnberg, D. Quaternary deep-thermocline cooling enhanced by southern Pacific Ocean tunnelling. *Commun. Earth Environ.* 6, 822 (2025). https://doi.org/10.1038/s43247-025-02886-x
23. Talley, L. D., Pickard, G. E., Emery, W. J. & Swift, J. H. *Descriptive Physical Oceanography: An Introduction*. 6th edn, pp. 303–362 (Elsevier, 2011).

24. Schneider, B. & Schmittner, A. Simulating the impact of the Panamanian seaway closure on ocean circulation, marine productivity and nutrient cycling. *Earth Planet. Sci. Lett.* 246, 367–380 (2006). https://doi.org/10.1016/j.epsl.2006.04.028
25. Sosdian, S. M. & Lear, C. H. Initiation of the Western Pacific warm pool at the middle Miocene climate transition? *Paleoceanogr. Paleoclimatol.* 35, e2020PA003920 (2020). https://doi.org/10.1029/2020PA003920
26. Zhang, Y. G., Pagani, M. & Liu, Z. A 12-million-year temperature history of the tropical Pacific Ocean. *Science* 344, 84–87 (2014). https://doi.org/10.1126/science.1246172
27. De Vleeschouwer, D., Lyu, J., Bialik, O. M., Christensen, B. A., Auer, G. & Batenburg, S. J. Pacific–Indian Ocean intermediate water exchange since the Middle Miocene: from Indonesian Throughflow to Tasman Leakage. *Paleoceanogr. Paleoclimatol.* 40, e2025PA005169 (2025). https://doi.org/10.1029/2025PA005169
28. Bali, H. & Gupta, A. K. Ocean gateways and circulation dynamics: unveiling the deep water-mass properties in the western equatorial Pacific since the Middle Miocene. *Mar. Micropaleontol.* 193, 102420 (2024). https://doi.org/10.1016/j.marmicro.2024.102420
29. Yamasaki, M., Tokumoto, R., Sasaki, A., Shimada, C. & Schiebel, R. Western to central equatorial Pacific planktic foraminiferal fluxes: implication for the relationship between their assemblage and warm pool migration from 1999 to 2002. *J. Foraminiferal Res.* 52, 140–159 (2022). https://doi.org/10.2113/gsjfr.52.3.140
30. Watkins, J. M., Mix, A. C. & Wilson, J. Living planktic foraminifera: tracers of circulation and productivity regimes in the central equatorial Pacific. *Deep Sea Res. Part II Top. Stud. Oceanogr.* 43, 1257–1282 (1996). https://doi.org/10.1016/0967-0645(96)00008-2
31. Gupta, A. K., Singh, R. K., Joseph, S. & Thomas, E. Indian Ocean high-productivity event (10–8 Ma): linked to global cooling or to the initiation of the Indian monsoons? *Geology* 32, 753–756 (2004). https://doi.org/10.1130/G20662.1
32. Pillot, Q., Suchéras-Marx, B., Sarr, A. C., Bolton, C. T. & Donnadieu, Y. A global reassessment of the spatial and temporal expression of the late Miocene biogenic bloom. *Paleoceanogr. Paleoclimatol.* 38, e2022PA004564 (2023). https://doi.org/10.1029/2022PA004564
33. Hodell, D. A. & Venz-Curtis, K. A. Late Neogene history of deepwater ventilation in the Southern Ocean. *Geochem. Geophys. Geosyst.* 7, Q09001 (2006). https://doi.org/10.1029/2005GC001211
34. Farrell, J. W., Raffi, I., Janecek, T. R., Murray, D. W., Levitan, M., Dadey, K. A. *et al.* Late Neogene sedimentation patterns in the eastern equatorial Pacific Ocean. In *Proceedings of the Ocean Drilling Program, Scientific Results* 138, 2419–2426 (Ocean Drilling Program, 1995). https://doi.org/10.2973/odp.proc.sr.138.143.1995
35. Filippelli, G. M. Intensification of the Asian monsoon and a chemical weathering event in the late Miocene–early Pliocene: implications for late Neogene climate change. *Geology* 25, 27–30(1997). https://doi.org/10.1130/0091-7613(1997)025%3C0027:IOTAMA%3E2.3.CO;2

36. Gastaldello, M. E. Unravelling changes in the productivity regime during the Late Miocene-Early Pliocene Biogenic Bloom: insights from the western equatorial Pacific (IODP Site U1488). *Mar. Micropaleontol.* 191, 102395 (2024). https://doi.org/10.1016/j.marmicro.2024.102395

37. Drury, A. J., Liebrand, D., Westerhold, T., Beddow, H. M., Hodell, D. A., Rohlfs, N. *et al.* Climate, cryosphere and carbon cycle controls on Southeast Atlantic orbital-scale carbonate deposition since the Oligocene (30–0 Ma). *Clim. Past* 17, 2091–2117 (2021). https://doi.org/10.5194/cp-17-2091-2021

38. Si, W. & Rosenthal, Y. Reduced continental weathering and marine calcification linked to late Neogene decline in atmospheric CO_2. *Nat. Geosci.* 12, 833–838 (2019). https://doi.org/10.1038/s41561-019-0450-3

39. Zhang, L., Chen, M., Xiang, R., Zhang, L. & Lu, J. Productivity and continental denudation history from the South China Sea since the late Miocene. *Mar. Micropaleontol.* 72, 76–85 (2009). https://doi.org/10.1016/j.marmicro.2009.03.006

40. Cook, C. P., Van De Flierdt, T., Williams, T., Hemming, S. R., Iwai, M., Kobayashi, M. *et al.* Dynamic behaviour of the East Antarctic ice sheet during Pliocene warmth. *Nat. Geosci.* 6, 765–769 (2013). https://doi.org/10.1038/ngeo1889

41. Miller, K. G., Kominz, M. A., Browning, J. V., Wright, J. D., Mountain, G. S., Katz, M. E. et al. The Phanerozoic record of global sea-level change. *Science* 310, 1293–1298 (2005). https://doi.org/10.1126/science.1116412

42. Coale, K. H., Fitzwater, S. E., Gordon, R. M., Johnson, K. S. & Barber, R. T. Control of community growth and export production by upwelled iron in the equatorial Pacific Ocean. *Nature* 379, 621–624 (1996). https://doi.org/10.1038/379621a0

43. Ryan, J. P., Ueki, I., Chao, Y., Zhang, H., Polito, P. S. & Chavez, F. P. Western Pacific modulation of large phytoplankton blooms in the central and eastern equatorial Pacific. *J. Geophys. Res. Biogeosci*. 111, G02013 (2006).https://doi.org/10.1029/2005JG000084.

44. Lyle, M., Dadey, K. A. & Farrell, J. W. The Late Miocene (11–8 Ma) Eastern Pacific carbonate crash: evidence for reorganization of deep-water circulation by the closure of the Panama Gateway. In *Proceedings of the Ocean Drilling Program, Scientific Results* 138 (Ocean Drilling Program, 1995). https://doi.org/10.2973/odp.proc.sr.138.157.1995

45. Gupta, A. K., Yuvaraja, A., Prakasam, M., Clemens, S. C. & Velu, A. Evolution of the South Asian monsoon wind system since the late Middle Miocene. *Palaeogeogr. Palaeoclimatol. Palaeoecol.* 438, 160–167 (2015). https://doi.org/10.1016/j.palaeo.2015.08.00

46. Holbourn, A. E., Kuhnt, W., Clemens, S. C., Kochhann, K. G., Jöhnck, J., Lübbers, J. & Andersen, N. Late Miocene climate cooling and intensification of southeast Asian winter monsoon. *Nat. Commun.* 9, 1584 (2018). https://doi.org/10.1038/s41467-018-03950-1

47. Mohanty, R. N., Gupta, A. K. & Clemens, S. Benguela upwelling system triggered and intensified southern African aridification in the Late Miocene. *Commun. Earth Environ.* 6, 989 (2025). https://doi.org/10.1038/s43247-025-02948-0

48. Westerhold, T., Marwan, N., Drury, A. J., Liebrand, D., Agnini, C., Anagnostou, E. *et al.* An astronomically dated record of Earth's climate and its predictability over the last 66 million years. *Science* 369, 1383–1387 (2020). https://doi.org/10.1126/science.aba6853
49. Vincent, E., Killingley, J. S. & Berger, W. H. Miocene oxygen and carbon isotope stratigraphy of the tropical Indian Ocean. (1985). doi: 10.1130/MEM163-p103
50. Tzanova, A., Herbert, T. D. & Peterson, L. Cooling Mediterranean Sea surface temperatures during the Late Miocene provide a climate context for evolutionary transitions in Africa and Eurasia. *Earth Planet. Sci. Lett.* 419, 71–80 (2015). https://doi.org/10.1016/j.epsl.2015.03.016
51. Seki, O., Schmidt, D. N., Schouten, S., Hopmans, E. C., Sinninghe Damsté, J. S. & Pancost, R. D. Paleoceanographic changes in the Eastern Equatorial Pacific over the last 10 Myr. *Paleoceanography* 27, PA3224 (2012). https://doi.org/10.1029/2011PA002158
52. Lawrence, K. T., Sigman, D. M., Herbert, T. D., Riihimaki, C. A., Bolton, C. T., Martinez-Garcia, A. *et al.* Time-transgressive North Atlantic productivity changes upon Northern Hemisphere glaciation. *Paleoceanography* 28, 740–751 (2013). https://doi.org/10.1002/2013PA002546
53. Lea, D. W. Not so permanent El Niño. *Science* 344, 52–53 (2014). https://doi.org/10.1126/science.1252246
54. Bartoli, G., Hönisch, B. & Zeebe, R. E. Atmospheric CO_2 decline during the Pliocene intensification of Northern Hemisphere glaciations. *Paleoceanography* 26, PA4213 (2011). https://doi.org/10.1029/2010PA002055
55. Pagani, M., Liu, Z., LaRiviere, J. & Ravelo, A. C. High Earth-system climate sensitivity determined from Pliocene carbon dioxide concentrations. *Nat. Geosci.* 3, 27–30 (2010) https://doi.org/10.1038/ngeo724
56. Haywood, A. M., Valdes, P. J. & Sellwood, B. W. Global scale palaeoclimate reconstruction of the middle Pliocene climate using the UKMO GCM: initial results. *Glob. Planet. Change* 25, 239–256 (2000). https://doi.org/10.1016/S0921-8181(00)00028-X
57. Ravelo, A. C., Andreasen, D. H., Lyle, M., Olivarez Lyle, A. & Wara, M. W. Regional climate shifts caused by gradual global cooling in the Pliocene epoch. *Nature* 429, 263–267 (2004). https://doi.org/10.1038/nature02567
58. Brierley, C. M., Fedorov, A. V., Liu, Z., Herbert, T. D., Lawrence, K. T. & LaRiviere, J. P. Greatly expanded tropical warm pool and weakened Hadley circulation in the early Pliocene. *Science* 323, 1714–1718 (2009). https://doi.org/10.1126/science.1167625
59. Christensen, B. A., Renema, W., Henderiks, J., De Vleeschouwer, D., Groeneveld, J., Castañeda, I. S. *et al.* Indonesian Throughflow drove Australian climate from humid Pliocene to arid Pleistocene. *Geophys. Res. Lett.* 44, 6914–6925 (2017). https://doi.org/10.1002/2017GL072977
60. Sun, D., Su, R., Bloemendal, J. & Lu, H. Grain-size and accumulation rate records from Late Cenozoic aeolian sequences in northern China: implications for variations in the East Asian winter monsoon and westerly atmospheric circulation. *Palaeogeogr. Palaeoclimatol. Palaeoecol.* 264, 39–53 (2008). https://doi.org/10.1016/j.palaeo.2008.03.011

61. Shi, J., Jia, Q., Nürnberg, D., Li, T., Xiong, Z. & Qin, B. Coupled nutricline and productivity variations during the Pliocene in the western Pacific warm pool and their paleoceanographic implications. *Glob. Planet. Change* 212, 103810 (2022). https://doi.org/10.1016/j.gloplacha.2022.103810
62. Kimble, K. & Herbert, T. Oceanic tunnel controls of eastern equatorial Pacific surface temperature and productivity over the past 3.6 Myr. *Geophys. Res. Lett.* 51, e2024GL112815 (2024). https://doi.org/10.1029/2024GL112815
63. Etourneau, J., Ehlert, C., Frank, M., Martinez, P. & Schneider, R. Contribution of changes in opal productivity and nutrient distribution in the coastal upwelling systems to Late Pliocene/Early Pleistocene climate cooling. *Clim. Past* 8, 1435–1445 (2012). https://doi.org/10.5194/cp-8-1435-2012
64. Sigman, D. M., Jaccard, S. L. & Haug, G. H. Polar ocean stratification in a cold climate. *Nature* 428, 59–63 (2004). https://doi.org/10.1038/nature02357
65. Cane, M. A. & Molnar, P. Closing of the Indonesian seaway as a precursor to east African aridification around 3–4 million years ago. *Nature* 411, 157–162 (2001). https://doi.org/10.1038/35075500
66. Lawrence, K. T., Pearson, A., Castañeda, I. S., Ladlow, C., Peterson, L. C. & Lawrence, C. E. Comparison of late Neogene Uk' 37 and TEX86 paleotemperature records from the eastern equatorial Pacific at orbital resolution. *Paleoceanography and Paleoclimatology*, *35*(7), e2020PA003858 (2000). https://doi.org/10.1029/2020PA003858s
67. Karas, C., Nürnberg, D., Tiedemann, R. & Garbe-Schönberg, D. Pliocene climate change of the Southwest Pacific and the impact of ocean gateways. *Earth Planet. Sci. Lett.* 301, 117–124 (2011). https://doi.org/10.1016/j.epsl.2010.10.028
68. Krebs, U., Park, W. & Schneider, B. Pliocene aridification of Australia caused by tectonically induced weakening of the Indonesian throughflow. *Palaeogeogr. Palaeoclimatol. Palaeoecol.* 309, 111–117 (2011). https://doi.org/10.1016/j.palaeo.2011.06.002
69. Martínez-Garcia, A., Rosell-Melé, A., Jaccard, S. *et al.* Southern Ocean dust–climate coupling over the past four million years. *Nature* 476, 312–315 (2011). https://doi.org/10.1038/nature10310
70. Kroenke, L. W., Berger, W. H. & Janecek, T. R. Proc. ODP, *Init. Repts.* 130, 369–493 (Ocean Drilling Program, College Station, TX, 1991). https://doi.org/10.2973/odp.proc.ir.130.109.1991
71. Raffi, I., Wade, B. S., Pälike, H., Beu, A. G., Cooper, R., Crundwell, M. P. & Vernyhorova, Y. V. The Neogene period. In *Geologic Time Scale 2020* (ed. Gradstein, F. M. *et al.*) pp. 1141–1215 (Elsevier, 2020) https://doi.org/10.1016/B978-0-12-824360-2.00029-2
72. Hemleben, C., Spindler, M. & Anderson, O. R. Taxonomy and species features. In *Modern Planktonic Foraminifera*, pp. 8–32 (Springer, New York, 1989).
73. Kennett, J. P. & Srinivasan, M. S. *Neogene Planktonic Foraminifera* (Hutchinson Ross Publishing Company, Stroudsburg, 1983).
74. Lam, A. & Leckie, R. M. Late Neogene and Quaternary diversity and taxonomy of subtropical to temperate planktic foraminifera across the Kuroshio Current Extension, northwest Pacific Ocean.

Micropaleontology 66, 177–268 (2020). https://doi.org/10.47894/mpal.66.3.01

75. Gupta, A. K. & Thomas, E. Initiation of Northern Hemisphere glaciation and strengthening of the northeast Indian monsoon: Ocean Drilling Program Site 758, eastern equatorial Indian Ocean. *Geology* 31, 47–50 (2003). https://doi.org/10.1130/0091-7613(2003)031%3C0047:IONHGA%3E2.0.CO;2
76. Aze, T., Ezard, T. H., Purvis, A., Coxall, H. K., Stewart, D. R., Wade, B. S. & Pearson, P. N. A phylogeny of Cenozoic macroperforate planktonic foraminifera from fossil data. *Biol. Rev.* 86, 900–927 (2011). https://doi.org/10.1111/j.1469-185X.2011.00178.x
77. Bé, A. W. H. & Tolderlund, D. S. Distribution and ecology of living planktonic foraminifera in surface waters of the Atlantic and Indian Oceans. In Funnell, B. M. & Riedel, W. R. (eds) *The Micropalaeontology of Oceans*, pp. 105–149 (Cambridge University Press, Cambridge, 1971).
78. Bé, A. W. An ecological, zoogeographic and taxonomic review of recent planktonic foraminifera. (1977).
79. Chaisson, W. Planktonic foraminiferal assemblages and palaeoceanographic change in the transtropical Pacific Ocean: a comparison of west (Leg 130) and east (Leg 138), latest Miocene to Pleistocene. In *Proc. ODP Sci. Results* 138, 555–597 (1995). https://doi.org/10.2973/odp.proc.sr.138.129.1995.
80. Douglas, R. G. & Savin, S. M. Oxygen isotopic evidence for the depth stratification of Tertiary and Cretaceous planktic foraminifera. *Mar. Micropaleontol.* 3, 175–196 (1978). https://doi.org/10.1016/0377-8398(78)90004-X
81. Keller, G. Depth stratification of planktonic foraminifers in the Miocene ocean. (1985). https://doi.org/10.1130/MEM163-p177
82. Anagnostou, E., John, E. H., Babila, T. L., Sexton, P. F., Ridgwell, A., Lunt, D. J. *et al.* Proxy evidence for state-dependence of climate sensitivity in the Eocene greenhouse. *Nat. Commun.* 11, 4436 (2020). https://doi.org/10.1038/s41467-020-17887-x
83. Brown, R. M., Chalk, T. B., Crocker, A. J., Wilson, P. A. & Foster, G. L. Late Miocene cooling coupled to carbon dioxide with Pleistocene-like climate sensitivity. *Nat. Geosci.* 15, 664–670 (2022). https://doi.org/10.1038/s41561-022-00982-7
84. De La Vega, E., Chalk, T. B., Wilson, P. A., Bysani, R. P. & Foster, G. L. Atmospheric CO_2 during the Mid-Piacenzian Warm Period and the M2 glaciation. Sci. Rep. 10, 11002 (2020). https://doi.org/10.1038/s41598-020-67154-8
85. Dyez, K. A., Hönisch, B. & Schmidt, G. A. Early Pleistocene obliquity-scale pCO_2 variability at ~ 1.5 million years ago. *Paleoceanogr. Paleoclimatol.* 33, 1270–1291 (2018). https://doi.org/10.1029/2018PA003349
86. Martínez-Botí, M. A., Foster, G. L., Chalk, T. B., Rohling, E. J., Sexton, P. F., Lunt, D. J. *et al.* Plio-Pleistocene climate sensitivity evaluated using high-resolution CO_2 records. *Nature* 518, 49–54 (2015). https://doi.org/10.1038/nature14145

87. Sosdian, S. M., Greenop, R., Hain, M. P., Foster, G. L., Pearson, P. N. & Lear, C. H. Constraining the evolution of Neogene ocean carbonate chemistry using the boron isotope pH proxy. *Earth Planet. Sci. Lett.* 498, 362–376 (2018). https://doi.org/10.1016/j.epsl.2018.06.017

88. Schlitzer, R. Ocean Data View. https://odv.awi.de (2022).

89. Zhang, S., Stier, P., Dagan, G. *et al.* Sea surface warming patterns drive hydrological sensitivity uncertainties. *Nat. Clim. Change* 13, 545–553 (2023). https://doi.org/10.1038/s41558-023-01678-5

90. Rousselle, G., Beltran, C., Sicre, M. A., Raffi, I. & De Rafélis, M. Changes in sea-surface conditions in the Equatorial Pacific during the middle Miocene–Pliocene as inferred from coccolith geochemistry. *Earth Planet. Sci. Lett.* 361, 412–421 (2013). https://doi.org/10.1016/j.epsl.2012.11.003.

91. Lukas, R. & Lindstrom, E. The mixed layer of the western equatorial Pacific Ocean. *J. Geophys. Res. Oceans* 96, 3343–3357 (1991). https://doi.org/10.1029/90JC01951

Figures

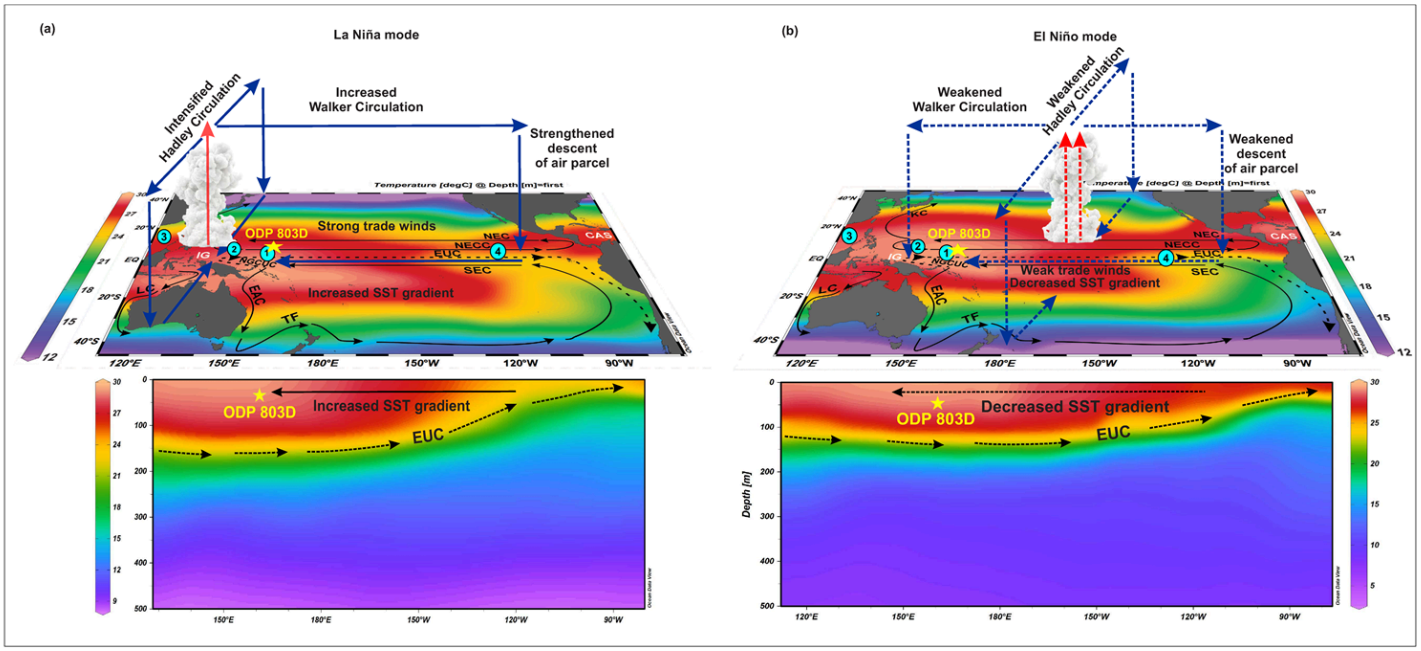

Figure 1

Conceptual schematic illustration of surface ocean–atmosphere interactions and major surface currents in the tropical Pacific. (a) La Niña-mode characterized by an increased sea surface temperature (SST) gradient, strengthened Walker and Hadley circulation. The lower panel shows a section of the upper 500 m of the water column at ODP Site 803, including depth and temperature along 2°N in the Pacific and an intensified Equatorial Undercurrent (EUC). (b) El Niño mode characterised by a decreased SST gradient, reduced Walker and Hadley circulations. The lower panel shows a section of the upper 500 m of the water column at ODP Site 803, including depth and temperature along 2°N in the Pacific and a weakened EUC. The base map was created using Ocean Data View (ODV)[88]. Surface currents are after Talley et

al.[23] (Black lines). Blue arrows indicate wind patterns; solid lines denoting strengthened winds (La Niña) and dashed lines denoting weakened winds (El Niño)[89]. The locations of sediment cores discussed in the study are marked as 1 = ODP Site 806[4,5,26] (WEP); 2 = IODP Site U1488[36] (WEP); 3 = ODP Site 1146[46] (South China Sea); 4 = IODP Site U1338[15] (East Equatorial Pacific). NEC: North Equatorial Current; NECC: North Equatorial Counter Current; SEC: South Equatorial Current; EUC: Equatorial Undercurrent (black dashed line); EAC: East Australian Current; KC: Kuroshio Current; LC: Leeuwin Current; NGCUC: New Guinea Coastal Undercurrent; TF: Tasman Front; IG: Indonesian Gateway; CAS: Central American Seaway from Talley et al.[23]. WEP = Western Equatorial Pacific.

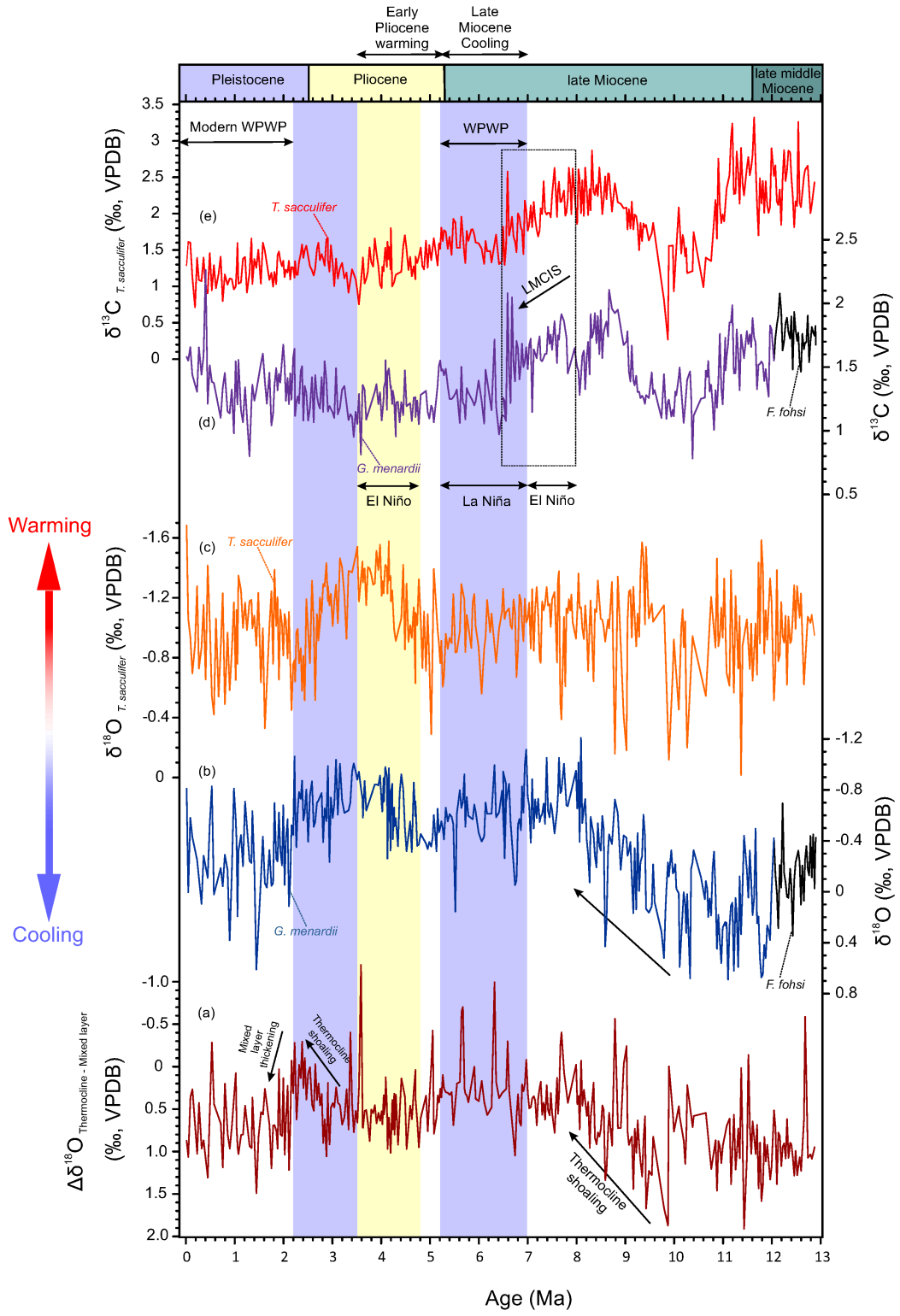

Figure 2

Proxy data from ODP Site 803. (a) $\Delta\delta^{18}O_{\text{Thermocline – Mixed layer}}$ (‰) (offset between the upper thermocline planktic foraminifer *F. fohsi* from ~12.9 Ma to 12.07 Ma; *G. menardii* from ~12.07 Ma to Present and mixed layer planktic foraminifer *T. sacculifer* from ~12.9 Ma to Present), (b) The $\delta^{18}O$ values of upper thermocline planktic foraminifera *G. menardii* are in navy blue and *F. fohsi* are in black. (c) The $\delta^{18}O$

values of mixed layer planktic foraminifer *T. sacculifer* are in orange, (d) The $\delta^{13}C$ values of upper thermocline planktic foraminifera *G. menardii* are in purple and *F. fohsi* in black, (e) The $\delta^{13}C$ values of mixed layer planktic foraminifer *T. sacculifer* are in red. LMCIS: Late Miocene Carbon Isotope Shift; WPWP: West Pacific Warm Pool. Yellow bars indicate periods of warming and blue bar represents the periods of cooling.

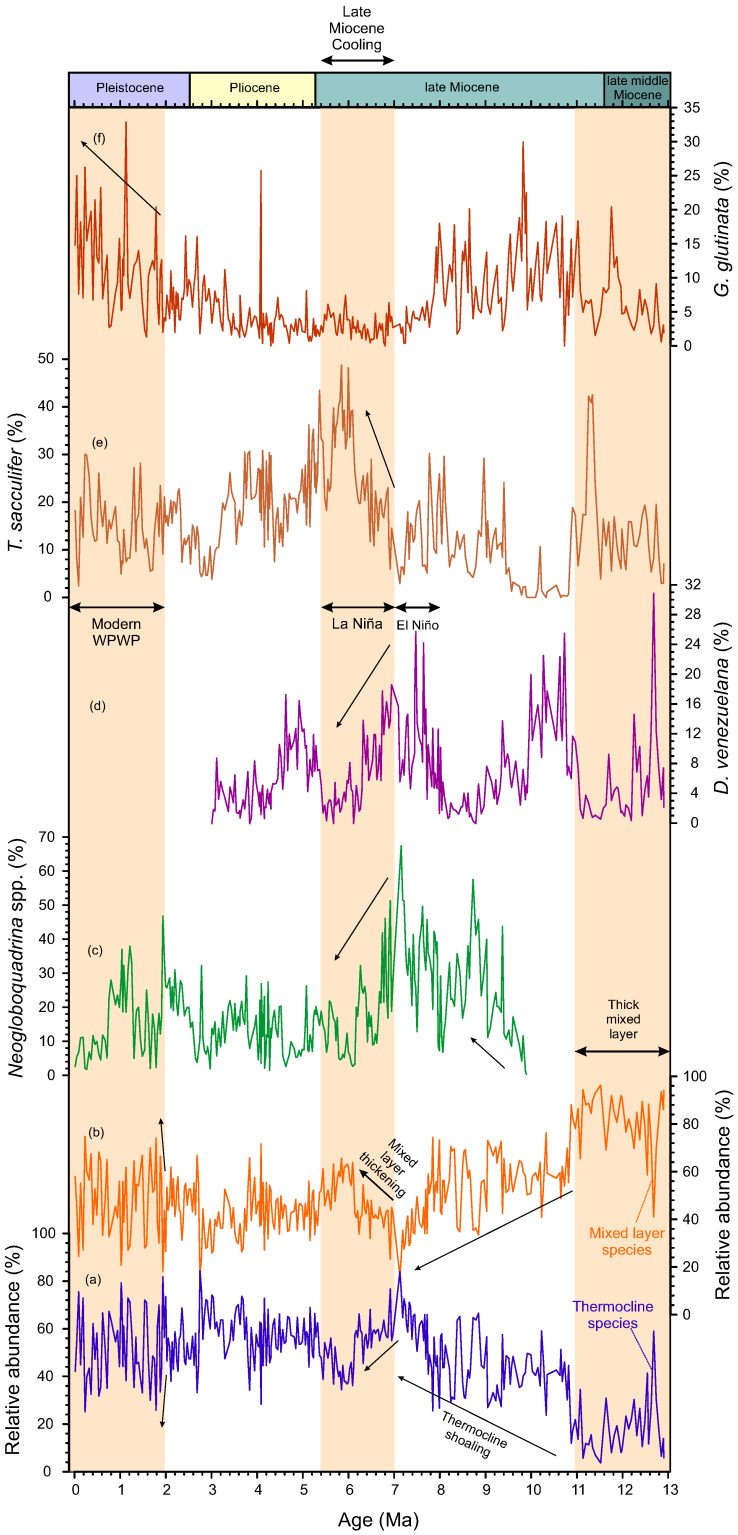

Figure 3

Proxy data from ODP Site 803. (a) Relative abundance of thermocline species (%), (b) Relative abundance of mixed layer species (%), (c) Relative abundance of *Neogloboquadrina* spp. (%), (d) Relative abundance of *D. venezuelana* (%), (e) Relative abundance of *T. sacculifer* (%), (f) Relative abundance of *G. glutinata* (%). Orange bars indicate intervals of thick mixed layer in the western equatorial Pacific representing strong West Pacific Warm Pool (WPWP).

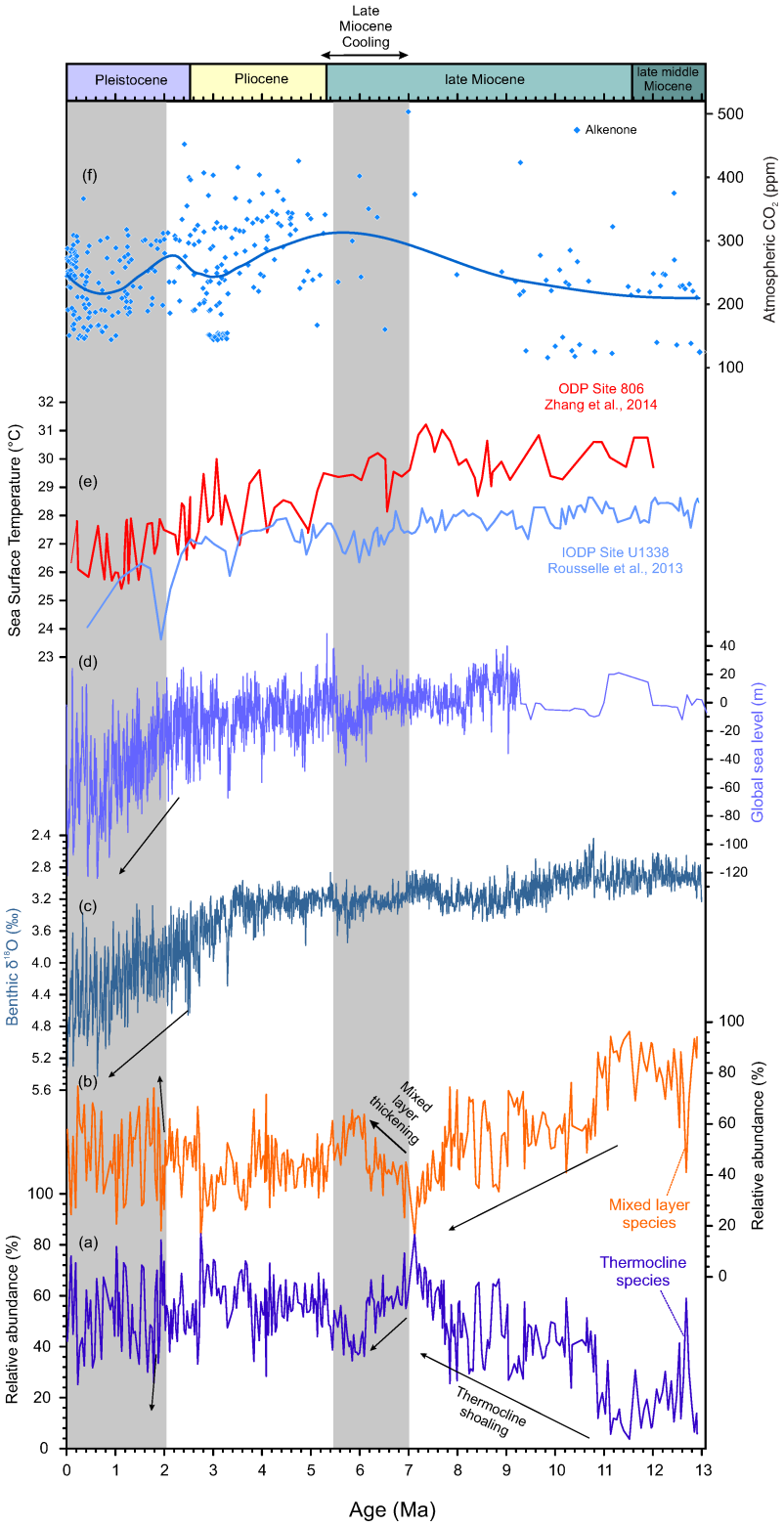

Figure 4

Comparison of proxy data from ODP Site 803 with previously published data from the Pacific. (a) Relative abundance of thermocline species (%) (this study), (b) Relative abundance of mixed layer species (%) (this study), (c) Global benthic foraminiferal oxygen isotope record from ~13 Ma to Present, derived from the CENOGRID dataset[48], (d) Global sea level variations from ~13 Ma to Present[41] , (e) Sea surface temperature (SST) records from western Pacific ODP Site 806 (*T. sacculifer* in red)[26] and eastern Pacific IODP Site U1338[90], (f) pCO_2 data compiled from numerous methodologies (https://paleo-co2.org) (references cited in Methods). Grey bars indicate periods of global cooling and falling sea level.

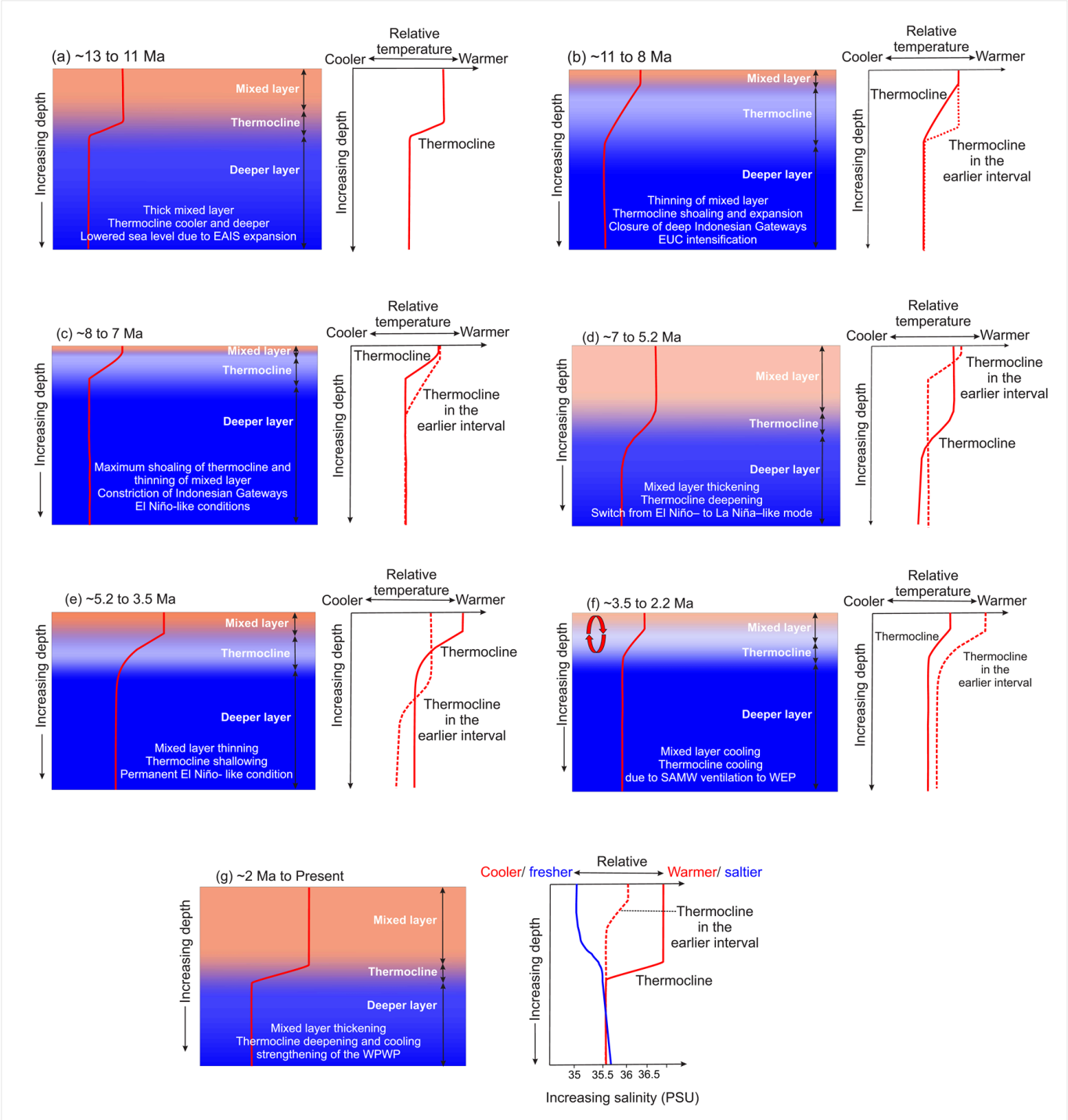

Figure 5

Schematic representation of upper ocean stratification and thermocline evolution in the western equatorial Pacific ODP Site 803 from ~13 Ma to the Present. (a) ~13 –11 Ma, (b) ~11– 8 Ma, (c) ~8 –7 Ma, (d) ~7 – 5.2 Ma, (e) ~5.2 – 3.5 Ma, (f) ~3.5 – 2.2 Ma, (g) ~2 Ma – Present. Arrows indicate relative changes in depth, and color gradients represent relative temperature variations, with blue denoting cooler and orange denoting warmer layers. The thermocline for a given interval is shown as a solid red line, whereas the dashed red line represents the thermocline position from the preceding interval. The blue line indicates the halocline in the most Recent interval. The salinity values are taken from Lukas and Lindstrom[91]. EAIS: East Antarctic Ice Sheet, EUC: Equatorial Undercurrent, LMC: Late Miocene Cooling, SAMW: Subantarctic Mode Water, WEP: Western equatorial Pacific, WPWP: West Pacific Warm Pool.

Supplementary Files

This is a list of supplementary files associated with this preprint. Click to download.

- supplementary.docx